Supplemental information

A novel reticular node in the brainstem synchronizes neonatal mouse crying with breathing

Xin Paul Wei, Matthew Collie, Bowen Dempsey, Gilles Fortin, Kevin Yackle

Corresponding author email: kevin.yackle@ucsf.edu

Inventory of Supplemental Information

1. Supplemental Figures
    - Figure S1, related to Figures 2, 4 and S7
    - Figure S2, related to Figure 2
    - Figure S3, related to Figure 3
    - Figure S4, related to Figure 3
    - Figure S5, related to Figure 6
    - Figure S6, related to Figure 6
    - Figure S7, related to Figures 6, 7
    - Figure S8, related to Figure 8

2. Supplemental Table
    - Table S1, related to Figure 8

3. Supplemental Video
    - Video S1, related to Figure 2 and S2

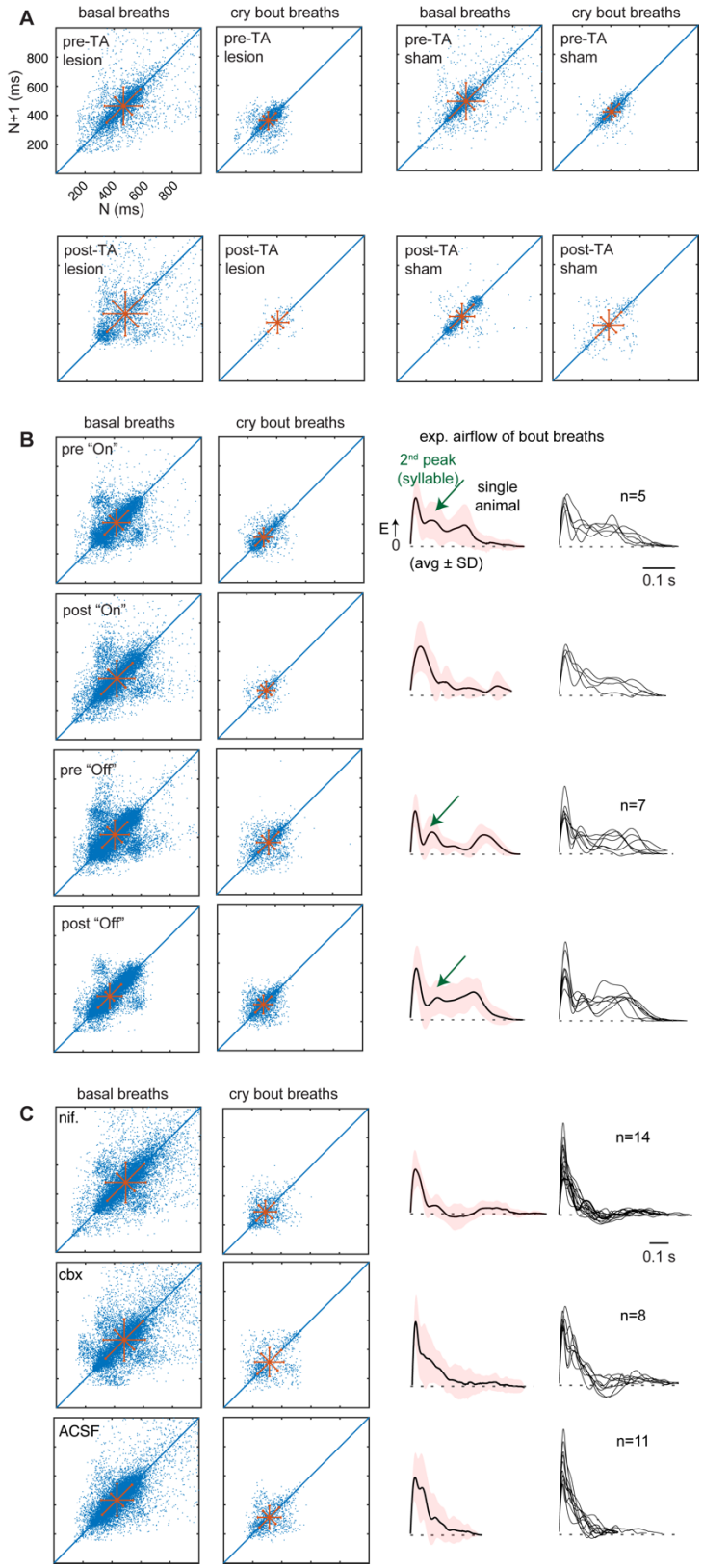
A
basal breaths
cry bout breaths
basal breaths
cry bout breaths
pre-TA lesion
pre-TA lesion
pre-TA sham
pre-TA sham
N+1 (ms)
800
600
400
200
200
400
600
800
N (ms)
post-TA lesion
post-TA lesion
post-TA sham
post-TA sham
B
basal breaths
cry bout breaths
exp. airflow of bout breaths
pre "On"
2nd peak (syllable)
single animal
n=5
E
0
(avg ± SD)
0.1 s
post "On"
pre "Off"
n=7
post "Off"
C
basal breaths
cry bout breaths
nif.
n=14
0.1 s
cbx
n=8
ACSF
n=11

Figure S1. Characterization of the basal and cry bout breathing rhythms in TA lesions, rv-iRF electrolytic lesions, and rv-iRF pharmacological injections. Related to Figures 2, 4, and S7. **A**, Poincaré plot of breath length (ms) for a breath (N) versus the subsequent breath (N+1) for basal (left) and cry bout (right) breaths before (top) and after (bottom) TA lesion or sham lesion. **B**, As in **A**, for breathing before and after on- and off-target electrolytic lesion of the rv-iRF. Right, representative cry breath expiratory airflow (average ± SD) from a single animal and the overlay of the average from all animals. Note, the cry breaths after the post on-target lose the second syllable airflow peak (green arrow). **C**, As in **B**, but following pharmacological injection of 10μM nifedipine, 1mM Cbx, or ACSF into the rv-iRF.

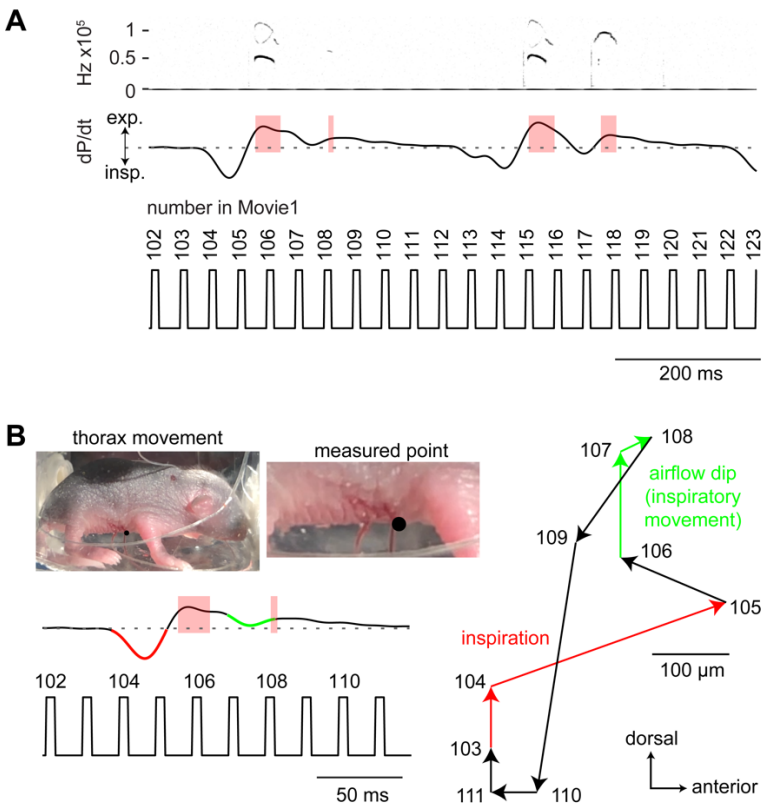

Figure S2. Breathing pressure changes and cries that correspond to the breathing movements in Video S1. Related to Figure 2. **A**, Spectrogram and respiratory pressure changes for two sequential breaths with bisyllabic cries. Numbers below correspond to Video S1 and are meant for alignment. Inspiration occurs in frames 103-105 and 113-115. Inspiratory-like events that separate each syllable occur in frames 106-107 and 116-118. **B**, Quantification of the thoracic body wall movements in Video S1. Black dot on the thorax represents the point tracked during the breath. As inspiration occurs, 103-105 (red), the thorax retracted (103-104) and moved anterior (104-105). This same movement, although smaller in magnitude, occurred during the inspiratory like event between the two syllables 106-108 (green). During expiration, the body wall relaxed (108-111). These body wall movements are consistent with the inspiratory motor program

measured in Figure 2 between syllables and demonstrates that the airflow oscillation between two syllables is likely generated by an inspiratory motor program.

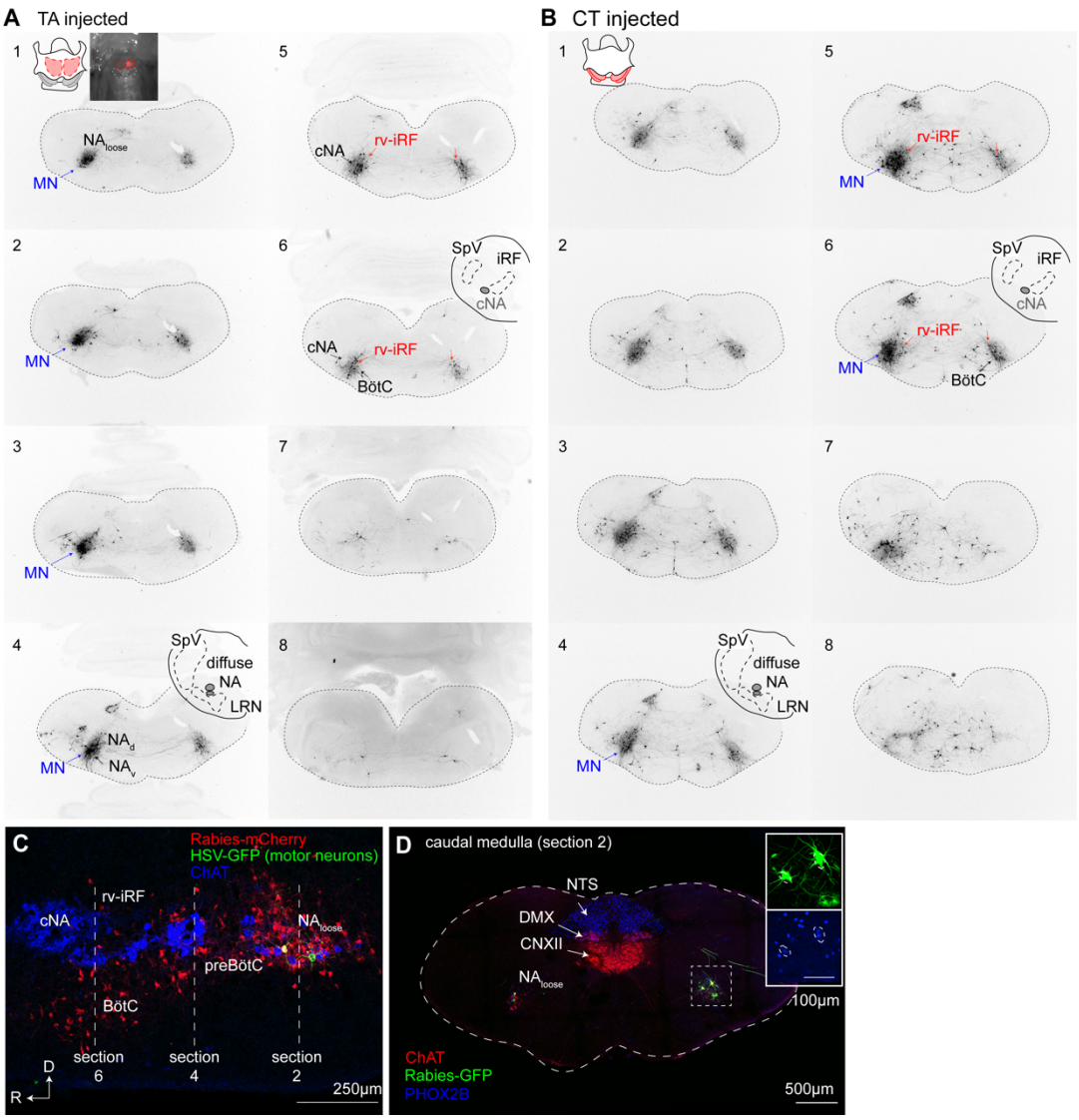

Figure S3. Complete medullary motor and premotor pattern from rabies-traced laryngeal muscles. Related to Figure 3. Sequential coronal sections of the medullary brainstem after ΔG rabies-tracing initiated unilaterally from the thyroarytenoid (TA, **A**) and the cricothyroid (CT, **B**) muscles. Sections are organized from caudal (1) to rostral (8). Red arrows in sections 5 and 6 indicate the anatomical location of rv-iRF. Note, rv-iRF neurons are premotor since they do not express Phox2b (Figure 3). Blue arrows indicate traced motor neurons (MN). These are identified by their large size and Phox2b

expression (Figures 3 and S3). Furthermore, their locations match the MN patterns identified by HSV-GFP (Figure S4), the absence of Vglut2 and Vgat expression (Figure 3), and the literature (Hernández-Morato et al., 2013). Black arrows indicate the loose formation of the nucleus ambiguus (NA_{loose}), semicompact (NA_d and NA_v), and compact (cNA). Black arrows on section 6 also indicate BötC. SpV, Spinal trigeminal nucleus. iRF, intermediate Reticular Formation. **C**, Sagittal section of the lateral medulla showing TA traced motor neurons after ΔG-rabies-mCherry and HSV-G-GFP microinjection. Motor neurons identified by HSV-Glycoprotein-GFP and ChAT expression (green and blue) and ΔG rabies-traced premotor neurons (red, rabies-mCherry positive, HSV-GFP negative, and ChAT negative). TA motor neurons are located in the NA_{loose}. C, caudal. D, dorsal. **D**, Example of coronal brainstem slice showing the thyroarytenoid (TA) motor neurons after ΔG-rabies-GFP microinjection. Motor neurons are identified by colocalization of ΔG rabies-GFP (green) Choline acetyl transferase immunostain (ChAT, red), and Phox2b immunostain (blue, shown below). Note, the TA motor neurons are in the NA_{loose} in the caudal brainstem where the NTS (nucleus tractus solitarius, Phox2b positive), DMX (dorsal motor nucleus 10, Phox2b and ChAT positive), and CNXII (cranial nerve 12, ChAT positive) are located.

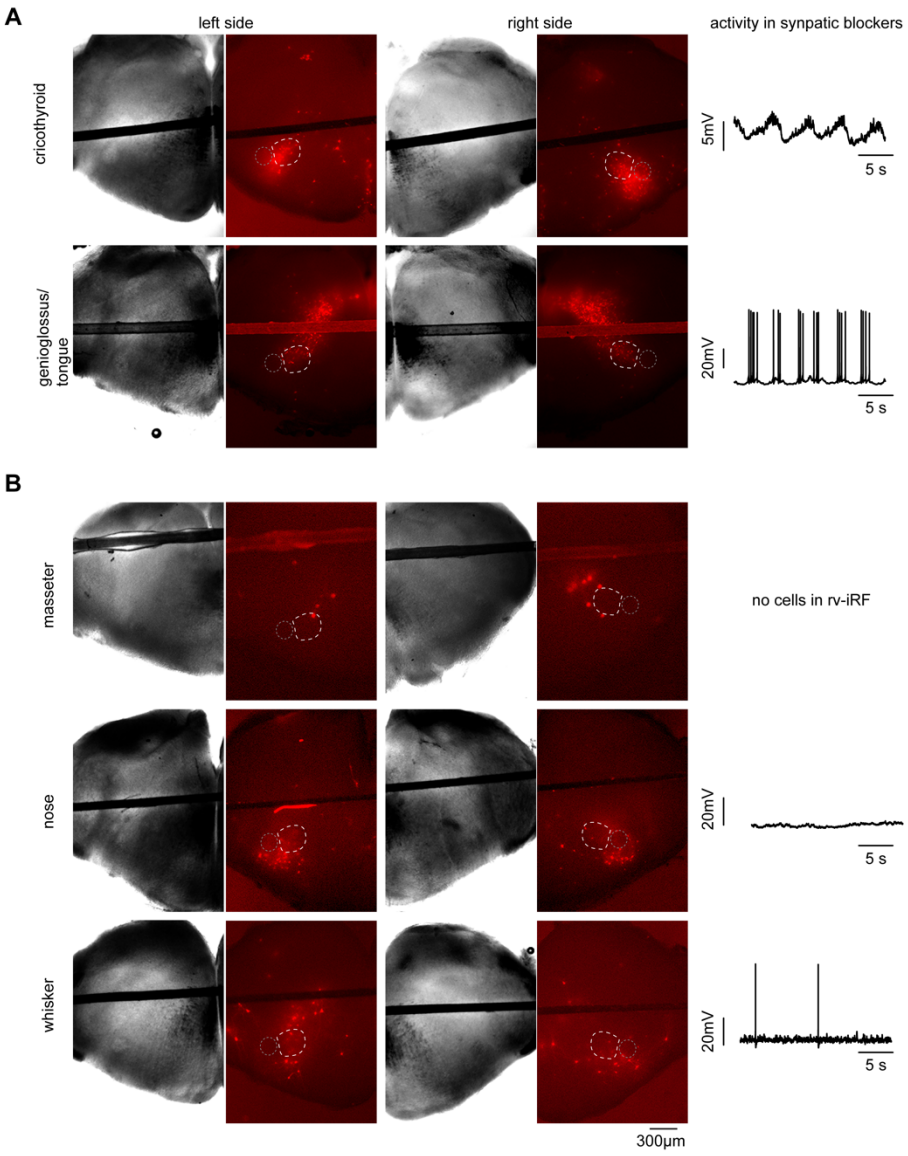

Figure S4. Anatomical location of rabies-traced premotor neurons from other orofacial muscles. Related to Figure 3. **A**, Left, Corresponding light and fluorescent microscopy images of the left and right sides of medullary brainstem slices depicting the location of the ΔG rabies-mCherry traced motor and premotor neurons (red) after injection of rabies into the cricothyroid and tongue. rv-iRF (dashed white), cNA (dashed gray). Right, Changes in membrane potential measured in current clamp of ΔG rabies neurons

in the rv-iRF in fast synaptic neurotransmission (10μM NBQX, 50μM APV, 100μM Picrotoxin, 1μM Strychnine). Oscillation in membrane potential indicates these neurons are within the iRO network (n = 7/19 for CT, n = 5/20 for tongue). **B**, As in A, but ΔG rabies-mCherry injected into other orofacial oscillators. Masseter (chewing, no neurons in rv-IRF), nose (sniffing, n = 0/6), and whisking (whisking, n = 0/5). The few neurons within rv-iRF did not display oscillations in membrane potential. Consistent with the coordination of nose movement and whisking with respiration, some rabies traced neurons localized to the preBötC/BötC, as has previously been described (Kurnikova et al., 2019; Moore et al., 2013; Stanek et al., 2014).

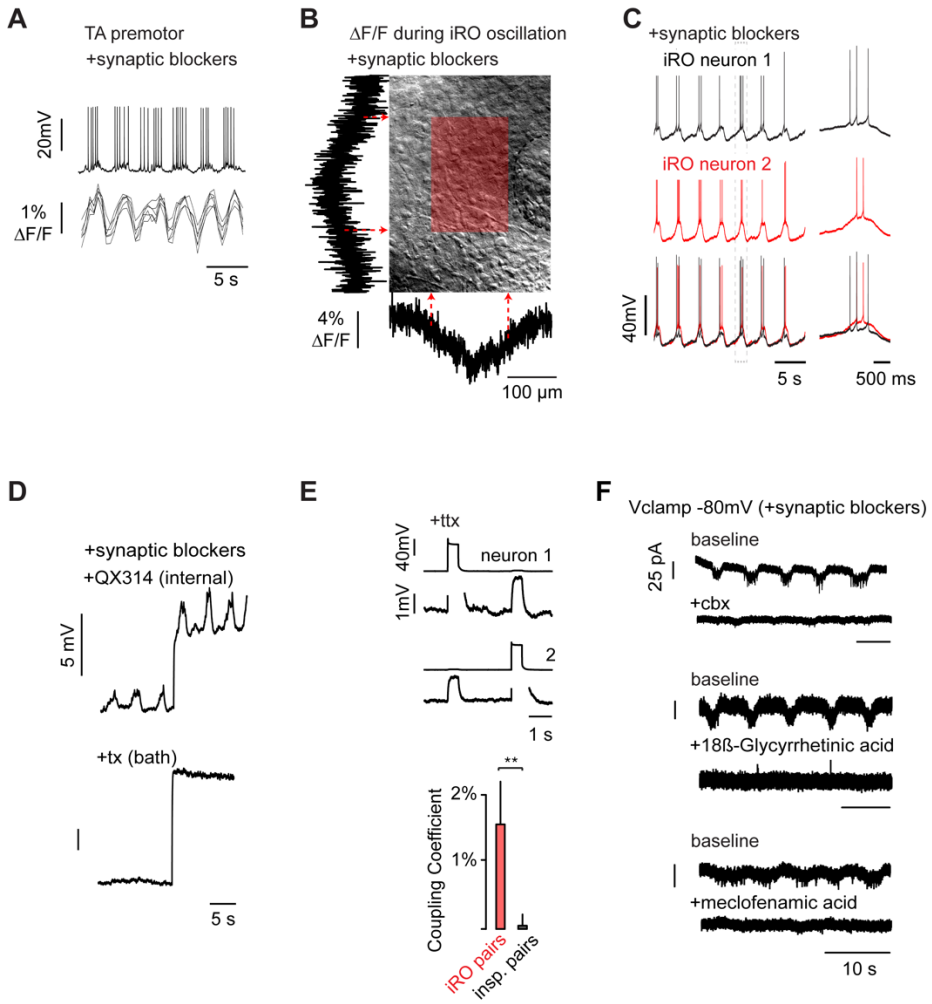

Figure S5. Gap junctions are required for the iRO rhythm. Related to Figure 6. **A**, I_c recording of TA premotor iRO neuron and ΔF/F in 6 iRO neurons (*Snap25*-GCaMP6s) with bath applied blockers of fast synaptic neurotransmission (10µM NBQX, 50µM APV, 100µM Picrotoxin, 1µM Strychnine). Synchronous rhythmic activity among iRO neurons persists. **B**, ΔF/F summed vertically and horizontally during a single oscillation in synaptic blocker. ΔF/F localizes to only dozens of neurons directly medial to cNA. **C**, Paired current clamp recordings of two iRO neurons in blockers of all fast synaptic neurotransmission (10µM NBQX, 50µM APV, 100µM Picrotoxin, 1µM Strychnine). N = 16. **D**, Current clamp

recording in fast synaptic blockers. Top, internal solution with QX314 (5mM). Bottom, same cell after bath application of tetrodotoxin (bottom, 1μM, n = 4). **E**, Paired I_c recordings of iRO neurons in 1μM TTX. 500 picoamp current injection into neuron 1 then neuron 2. Right, Coupling coefficient (∆mV uninjected / ∆mV injected) for iRO and control inspiratory neuron pairs. iRO coupling coefficient 1.2 ± 1.4%, n = 8; control inspiratory 0.00 ± 0.6%, n = 4. T-test P-value = 0.007. **I**, Voltage clamp recording of iRO neuron at -80 mV with synaptic blockers then with the gap junction antagonists 100 μM carbenoxolone (n = 12), 18ß-glycyrrhetinic acid (150μM, n = 2) and meclofenamic acid (100μM, n = 4).

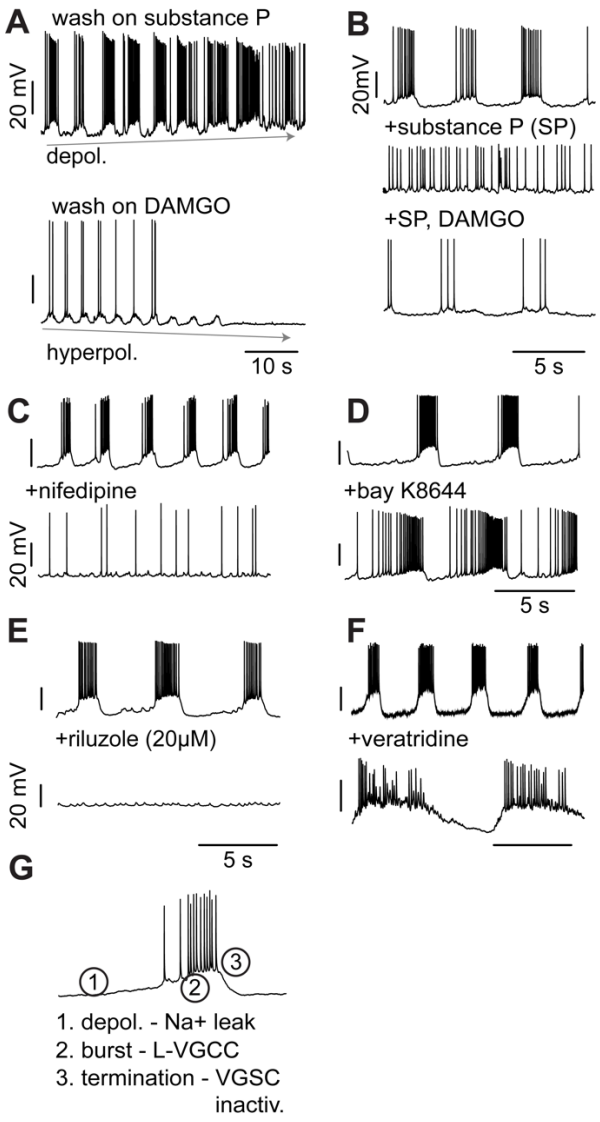

Figure S6. The iRO rhythm is voltage dependent. Related to Figure 6. **A**, iRO rhythm in fast synaptic blockers during bath application of the depolarizing neuromodulator Substance P (200nM, top) or hyperpolarizing neuromodulator DAMGO (200nM, bottom). **B**, Top, baseline. Middle, Substance P. Bottom, Substance P and DAMGO. **C**-**E**, Current clamp recording iRO neurons in fast synaptic blockers at baseline (top) and after bath application of nifedipine (**C**, 2μM), Bay K8644 (**D**, 100nM), Riluzole (**E**, 20μM), and veratridine (**F**, 250nM). Note, baseline rhythm varies from slice to slice, but each neuron

was confirmed to be part of the iRO gap junctioned network based on retained rhythmic activity in fast synaptic blockers. **G**, Model for molecular basis of iRO rhythm. Na^+ leak channels depolarize the network until VGSC spiking occurs (1) which is converted into a burst by L-type voltage gated calcium channels (2). The burst is terminated by inactivation of VGSCs (3).

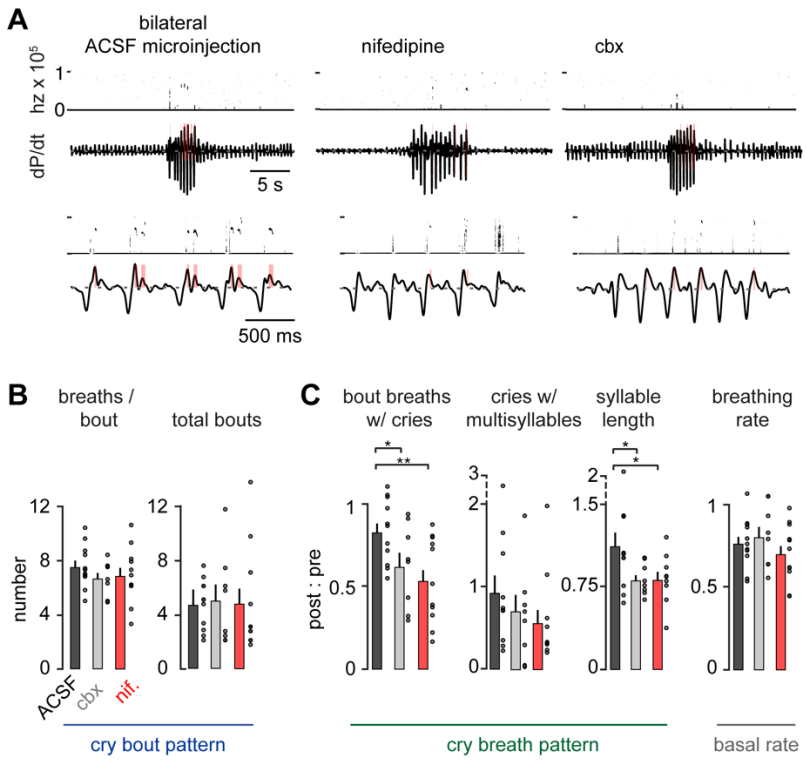

Figure S7. The iRO's intrinsic oscillation is required for cries but not breathing. Related to Figures 6 and 7. **A**, Representative cry bout (top) and breaths within (bottom) after bilateral iRO microinjection of 70nL artificial cerebrospinal fluid (ACSF), 10μM nifedipine, or 1mM Cbx. **B**, Total number of cry bouts and breaths within each bout after microinjection of ACSF (n=11), nifedipine (n=11), or carbenoxolone (n=8). **C**, As in Figure 4. Post-injection : pre-injection values for the cry breaths with cry vocalizations, multisyllabic cries, cry syllable lengths, and basal breathing. Data are mean ± SEM. One-sided t-test or Wilcoxon rank sum P-value < 0.05 (*) and < 0.01 (**).

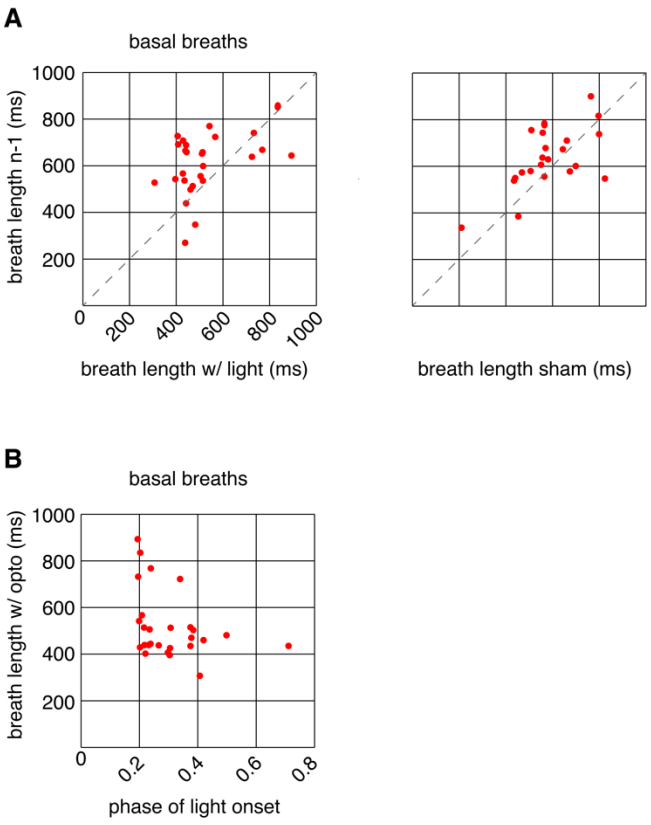

Figure S8. The iRO's intrinsic oscillation is required for cries but not breathing. Related to Figure 8. **A**, Left, comparison of basal breath rate with 50 ms light stimulation (x-axis, breath w/ light) versus the preceding breath (n-1). Right, sham basal breath versus n-1. **B**, Phase of breath at the onset of the 50 ms pulse (x-axis) versus the breath length. Note that the light pulse does not shift the length of the breath.

Table S1. iRO activity in transgenic Cre-induced GCaMP6 lines that label different neural types and compartments of the respiratory neural network. Related to Figure 8.

Allele	iRO	Respiratory brainstem compartment	
Vglut2-cre	yes	Glutamatergic	n=4
Gad2-cre	no	Inhibitory	n=4
Vgat-cre	no	Inhibitory	n=3
Glyt2-cre	no	Inhibitory	n=8
RIKEN-Glyt2-cre	no	Inhibitory	n=2
Chat-cre	no	PiCo	n=8
Dbx1-cre	yes	preBötC	n=3
Foxp2-cre	no	preBötC	n=8
Egr2-cre	no	Embryonic parafacial	n=2
Neurod6-cre	no	BötC	n=2
Penk-cre	yes	Neuropeptide	n=1
Parv-cre	no	BötC	n=1
Tac1-cre	yes	Neuropeptide	n=1
NPY-cre	no	A1/C1	n=1

Video S1. The changes in breathing movements related to cries in figure S2. **Related to Figure 2.** Neonatal mouse in plethysmograph and ultrasonic vocalization recording chamber. Video shows two breaths that each contain a bisyllabic cry. See Figure S1 for airflow trace and spectrogram. Numbers correspond to the numbers underlying the trace to Figure S1. These are used to align the time in the Video with Figure S1. Note, as the animal inspires the chest/abdomen retract, the head moves forward, and the mouth opens (examples 104-106 and 113-115). During the gap between the two syllables, the same movements are observed (examples 107-109 and 116-118). Thoracic body wall movements trajectories in Figure S1. The body movements and EMG recordings (Figure 2) are consistent with the airflow oscillation between two syllables being generated by an inspiratory motor program.